arXiv:astro-ph/9903438v1 29 Mar 1999

GRB990123: The Case for Saturated Comptonization

E. P. Liang, A. Crider, M. Böttcher, & I.A. Smith
Department of Space Physics and Astronomy, 6100 S. Main, Rice University, Houston, TX 77005-1892

ABSTRACT

We find that the optical magnitudes of GRB990123 observed by ROTSE correlates with the magnitudes extrapolated from the simultaneous BATSE spectra, strongly suggesting that the optical, X-ray and gamma-ray photons originate from a single source. We then show that the broadband optical-gamma-ray spectra can be naturally fit by the saturated Compton model. We also derive the parameters of the Compton emitting shell from first principles.

Subject headings: gamma-ray: bursts, observations

1. Introduction

The recent simultaneous detection of optical (Akerloff et al. 1999), X-ray (Feroci et al. 1999) and gamma-ray (Kippen et al. 1999) photons from GRB990123 during the burst provides the first broadband multi-wavelength characterization of the burst spectrum and evolution. Here we show that a direct correlation exists between the time-varying gamma-ray spectral shape and the prompt optical emission. This combined with the unique signatures of the time-resolved spectra of GRB990123 convincingly supports earlier predictions of the saturated Comptonization model (Liang et al. 1997, Liang 1997). Contrary to other suggestions (Galama et al. 1999, Sari & Piran 1999), we find that the entire continuum from optical to gamma-rays can be generated from a single source of leptons (electrons and pairs). The optical flux only appears to lag the gamma-ray flux due to the high initial Thomson depth of the plasma. Once the plasma has completely thinned out, the late time afterglow behavior of our model is the same as in standard models based on the Blandford-McKee (1976) solution.

2. Data Analysis and Interpretation

To generate the gamma-ray spectra of GRB990123 during the ROTSE observations, we fit the public BATSE data (SHER/SHERB+DISCSP1; see Preece et al. 1996) with the Band et al. (1993) GRB function, which is a four-parameter model that smoothly joins two power laws. Although the gamma-ray flux time history initially appears to be uncorrelated with the earliest observed optical evolution, a V-band extrapolation of the Band GRB function fit to the BATSE data shows a remarkable correlation with

the ROTSE fluxes (see Fig. 1). This suggests that the gamma-ray and optical emission likely arise from the same source. We stress that *it is essential to consider the time-varying shape of the GRB continuum and not the merely the magnitude of the γ-ray flux.*

Examination of the MER/CONT data during with the first ROTSE time bin, which includes approximately 10× as many counts as the SHER/SHERB data, shows an upturn in the lowest energy channel, inconsistent with the Band GRB function fit by 6.7σ. Inclusion of the SD discriminator channel corroborates the MER/CONT upturn and is inconsistent from the Band GRB function fit by 3.7σ. (We also find the discriminator channel data to be in rough agreement with the peak flux reported by BeppoSAX (Feroci et al. 1999), assuming a simple power-law spectra exists between the lowest MER channel and the ROTSE observations.) Fitting the MER+DISCSP1 spectra with a function which allows a low-energy upturn, such as the Compton attenuation function (Brainerd 1994, Brainerd et al. 1998), drastically improves the χ^2 of the fit by 143 without including extra degrees of freedom. Such upturns have been observed in many previous bursts (Fenimore, Klebesadel, Laros, & Stockdale 1982 , Brainerd et al. 1998, Crider et al. 1999), for example in GRB970111 using the joint BeppoSAX-BATSE spectrum (Crider et al. 1999). As we describe below, however, while the Compton attenuation model can mimic the observed gamma-ray spectra, it cannot produce the observed X-rays seen by BeppoSAX. We turn instead to inverse Comptonization spectra, which naturally produces both the "terrace" spectral shape seen by BATSE, the X-ray flux seen by BeppoSAX, and the optical flux seen by ROTSE. In Figure 2, we plot the three BATSE spectra deconvolved with inverse Comptonization spectra (see Section 3), as well as the simultaneous ROTSE optical measurements.

The popular optically thin synchrotron shock model for the relativistic blast wave (e.g. Mészáros & Rees 1993, Piran & Shemi 1993, Katz 1994, Tavani 1996) can only produce the high energy spectral break provided the slope below the break is $< -\frac{2}{3}$. It cannot produce the additional low energy upturn. To maintain the optically thin synchrotron shock model, it has been proposed that the optical emission comes from a separate component (Sari & Piran 1999). However, as we see in Fig. 1, a separate optical source is unnecessary and artificial given the correlation between the optical flux and the gamma-ray extrapolation. Moreover, the BATSE data alone in Fig. 2a is enough to establish the terrace shape. A separate problem with the synchrotron shock model is that it violates the observed spectral evolution seen in many bursts (Crider et al. 1997, Preece et al. 1998). A terrace can in principle be produced also by the Compton attenuation of a power law spectrum by cold intervening material (Brainerd et al. 1998, Brainerd 1994, Liang & Kargatis 1994). However, the extremely high column density ($N_H > 10^{25}$ cm^{-2}) required, even for sub-solar abundances of metals, would have completely absorbed the < 10 keV X-rays, contrary to the BeppoSAX results. For GRB990123 the required extinction would also be inconsistent with the blue color of

the optical source. Thus the broadband spectra of Fig. 2 are inconsistent with the Compton attenuation model.

The terrace shape continuum, such as that in Fig.2a, is a natural consequence and unique signature of saturated Comptonization (Rybicki & Lightman 1979, Sunyaev & Titarchuk 1980, Fenimore, Klebesadel, Laros, & Stockdale 1982) and was predicted two years ago when this model was developed to explain other details of GRB spectral evolution (Liang et al. 1997, Liang 1997). In this picture the GRB phase of a burst corresponds to the time when the relativistically expanding shell is still very dense and Thomson thick ($\tau_{\rm T} > 1$). *The X- and gamma-rays are produced by multiple Compton upscattering of self-emitted synchrotron and bremsstrahlung soft photons* (peaking below the IR; Liang 1997). When the Thomson depth is very high a Wien peak emerges producing a high-energy spectral break (Rybicki & Lightman 1979). At low energies, the spectrum turns up with a power-law of slope ≤ -1, producing the characteristic terrace shape (Fig. 2a & 3a). The low energy upturn usually occurs approximately one order of magnitude below the high energy break (Rybicki & Lightman 1979, Sunyaev & Titarchuk 1980, Liang & Nolan 1984). This low energy upturn is caused by the competition between spatial and energy diffusion in a medium with *volume* injection of soft photons. In the Compton cooling model (Liang et al. 1997), the photon diffusion time is assumed to be *shorter* than the observable burst evolution timescales. The typical "hard-to-soft" spectral evolution and pulse broadening with decreasing photon energy are then interpreted as due to the Compton cooling plus optical thinning of the emitting plasma. The above limit on the photon diffusion time puts constraints on the shell thickness and density. Details will be discussed elsewhere.

3. Monte Carlo Spectral Modeling

We have performed a systematic modeling of the three GRB990123 spectra using our Monte Carlo Compton code for hybrid thermal-nonthermal plasmas (Böttcher & Liang 1998). A thin uniform shell of thermal plus nonthermal leptons Compton upscatter self-emitted synchrotron and bremsstrahlung photons. The output is then Lorentz boosted and cosmologically redshifted to the observer frame to match the data. Hence the shell parameters are dependent on the bulk Lorentz factor which must be constrained from other physical self-consistency considerations (e.g. pulse rise times; Liang 1997). For a given Γ the Comptonized spectrum is then specified by the (comoving frame) magnetic field B, Thomson depth $\tau_{\rm T}$, thermal lepton temperature T, nonthermal lepton fraction ξ and nonthermal power law index p. We have used an upper Lorentz factor cutoff of 10^6 in the lepton distribution, which is adequate for modeling spectra up through the COMPTEL energy range.

Because of the large number of model parameters, the currently available spectral data is not very constraining on the model parameter space. Even if we had more

data points (e.g. from BeppoSAX, OSSE, and COMPTEL) computational limitations prohibit us from directly searching for the best fit model spectrum using chi-square minimization techniques. Hence the model fits presented here in Fig.2 are only meant to demonstrate a proof of principle, showing the resulting terrace shape and its evolution. Parameters of the sample model are listed in the caption of Figure 2. Even with such crude fits we can see evidence of Thomson thinning and steepening of the nonthermal lepton index.

In Fig.3 we show examples of different Monte Carlo Compton spectra to illustrate how the spectral shape varies with the different input parameters. We see that the prominence of the terrace is primarily correlated with the Thomson depth.

4. Compton Shell Parameters

We have deconvolved the time-resolved BATSE spectra for the whole burst using the Band et al. GRB function. The BATSE spectral evolution data allows us to derive the E_{pk}-fluence decay constant (Liang & Kargatis 1996, Crider et al. 1999) Φ_0 of each pulse. We find apparent $\Phi_0 \sim 150 - 300 \mathrm{cm}^{-2}$ for the pulses containing the three optical intervals (the intrinsic Φ_0 could be lower due to gravitational lensing). From this plus the pulse rise times we can constrain from first principles the Compton ejecta shell parameters (Liang 1997), including Γ, the shell radius, thickness, density, total leptonic mass M_e and total leptonic energies. These model parameters are listed in Table 1. Using these parameters we can estimate the transition time from the free-expansion (internal shock) phase to the blast wave (external shock) phase which is nominally identified with the "afterglow" power law, as a function of the ISM/CBM density and ejecta proton loading. We see that the predicted transition time to the afterglow phase (cf. Table 1) is indeed consistent with the observed transition time of a few hundred seconds (Galama et al. 1999).

This work was supported by NASA (NAG 5-3824). A.C. thanks MSFC for his NASA GSRP fellowship.

REFERENCES

Akerloff, C.W., et al. 1999, IAU Circ No. 7100

Band, D., et al. 1993, ApJ, 413, 281

Blandford, R. D. & McKee, C. F. 1976, Phys. Fluids 19, 1130-1138

Böttcher, M. & Liang, E.P. 1998, ApJ, 506, 281

Brainerd, J.J. 1998, ApJ, 501, 325

Brainerd, J.J. 1994, ApJ, 428, 21

Crider, A., et al. 1999, ApJ, 519

Crider, A., et al. 1999, BAAS, vol. 30, no. 4, 1380

Crider, A., et al. 1997, ApJ, 479, L39

Fenimore, E.E., Klebesadel, R.W., Laros, J.G., & Stockdale, R.E. 1982, Nature, 297, 665-667

Feroci, M., et al. 1999, IAU Circ. 7095

Galama, T.J., et al. 1999, Nature, (in press)

Katz, J.I. 1994, ApJ, 432, L107

Kippen, R.M., et al. 1999, GCN No. 224

Liang, E.P. 1997, ApJ, 491, L15

Liang, E.P., Smith, I.A., Kusunose, M., & Crider, A. 1997, ApJ, 479, L35

Liang, E.P. & Kargatis V.E. 1996, Nature, 381, 49

Liang, E.P. & Kargatis V.E. 1994, ApJ, 432, L111

Liang, E.P. & Nolan, P.L. 1984, Space Sci. Rev., 38, 353-384

Mészáros, P. & Rees M.J. 1993, ApJ, 405, 278

Piran, T. & Shemi, A. 1993, ApJ, 403, L67-L69

Preece, R.D. et al. 1998b, ApJ, 506, L23

Preece, R.D., et al. 1996, ApJ, 473, 310

Rybicki, G.B. and A.P. Lightman 1979, Radiative Processes in Astrophysics, (New York:Wiley)

Sari, R. & Piran, T. 1999, astro-ph/9902009

Sunyaev, R. & Titarchuk, L. 1980, A&A, 86, 121

Tavani, M. 1996, ApJ, 466, 768

This preprint was prepared with the AAS LaTeX macros v4.0.

Fig. 1.— The gamma-ray (24-1800 keV) and optical prompt emission of GRB990123. The gamma-ray photon flux is calculated from MER data fit using a Band et al. (1993) GRB function with β fixed to -3 (as found by OSSE). Extrapolating a Band GRB function fit to the SHER/SHERB data during each ROTSE time bin gives V magnitudes (plotted as squares). This shows a similar evolution to the ROTSE observations (plotted as circles). There are minor differences in the time intervals used due to binning constraints.

Fig. 2.— The BATSE spectra of GRB990123 coincident with the first three ROTSE observations. The dashed curves show the extrapolations of the Band (1993) GRB function fits to the gamma-ray data. The histograms show our Monte Carlo inverse Comptonization model spectra. The parameters used in each simulation are: (a) $\tau_{\rm T} = 20, {\rm kT}\ \Gamma/(1+{\rm z}) = 80$ keV, $\xi = 3\%, {\rm B} = 10^2$ G, ${\rm p} = 3$; (b) same parameters except $\tau_{\rm T} = 6$ and ${\rm p} = 6$; (c) same parameters except $\tau_{\rm T} = 8.4$ and ${\rm p} = 6$.

Fig. 3.— Compton spectra from a hybrid thermal-nonthermal plasma code (a) varying Thomson depth $\tau_{\rm T} = [10^{-5}({\rm A}), 1({\rm B}), 6({\rm C}), 20({\rm D})]$ with kT=5 keV, ξ=10%, B=10^3 G, and p=6. Note that the uncomptonized spectrum (curve A) is a superposition of synchrotron and bremsstrahlung source functions; (b) varying nonthermal fraction ξ = [3% (A), 5% (B), 10% (C)] with kT=5 keV, τ_T=8.4, B=10^3 G,and p=6. Note that the spectral break moves to higher energy as ξ is increased; (c) varying thermal temperature kT=[1 keV (A), 3 keV (B)] with τ_T=16, B=10^2 G, and p=3. Note that both the spectral break moves to higher energy and the spectrum gets harder as kT is increased; (d) varying nonthermal lepton index p=[6 (A), 2 (B)] with τ_T=6, kT=5 keV, B=10^3 G, and ξ=10%.

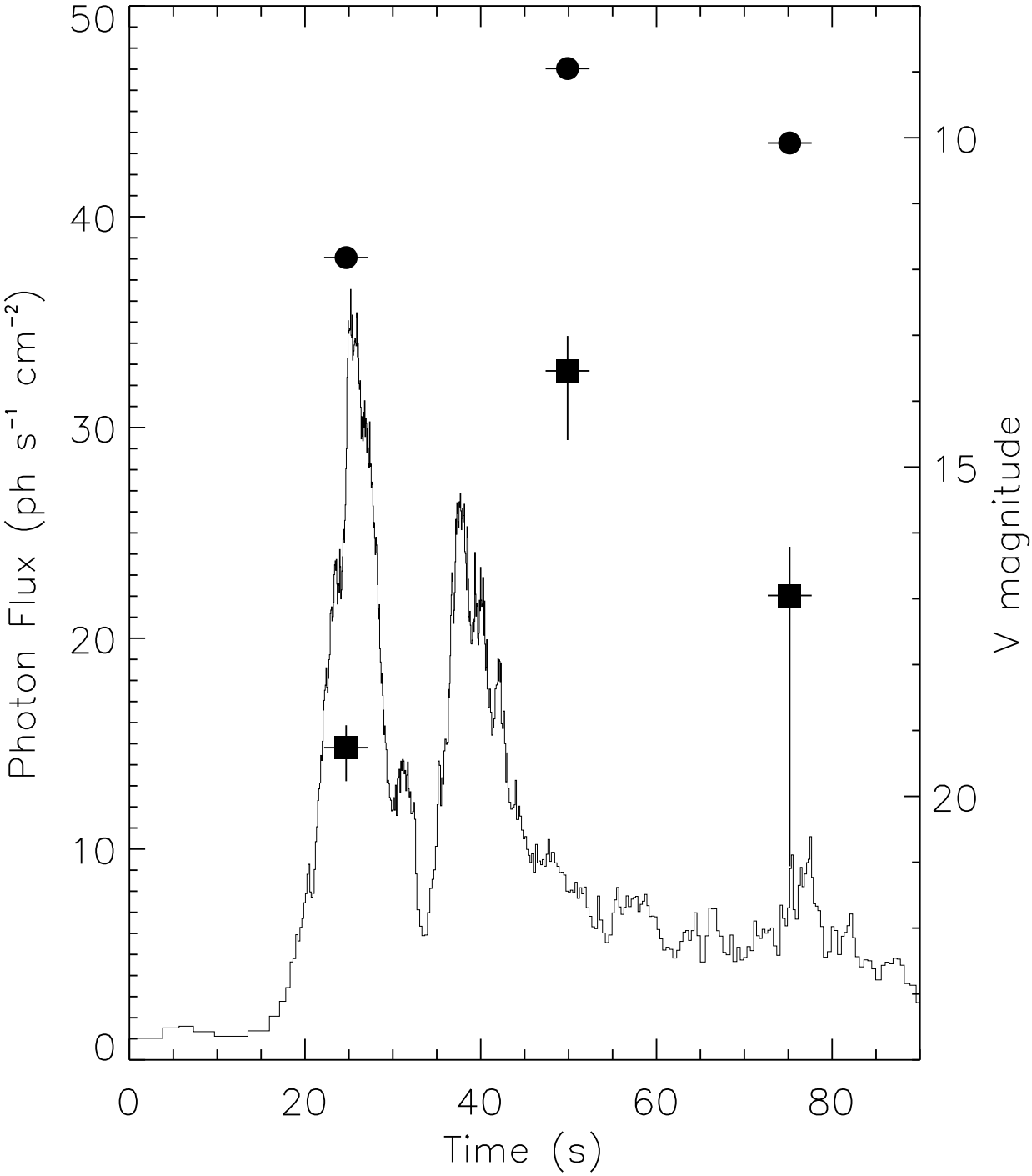
Photon Flux (ph s^{-1} cm^{-2})
V magnitude
Time (s)
0
10
20
30
40
50
0
20
40
60
80
10
15
20

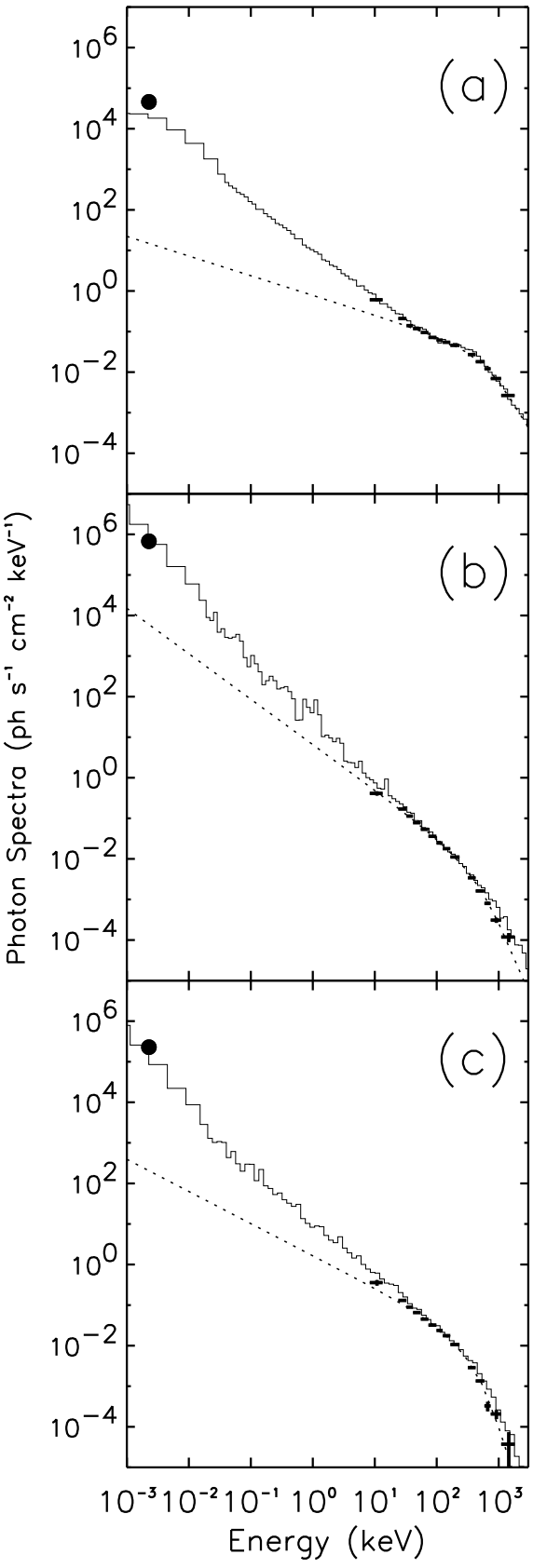
(a)
(b)
(c)
Photon Spectra (ph s⁻¹ cm⁻² keV⁻¹)
Energy (keV)
10⁻³ 10⁻² 10⁻¹ 10⁰ 10¹ 10² 10³
10⁶ 10⁴ 10² 10⁰ 10⁻² 10⁻⁴

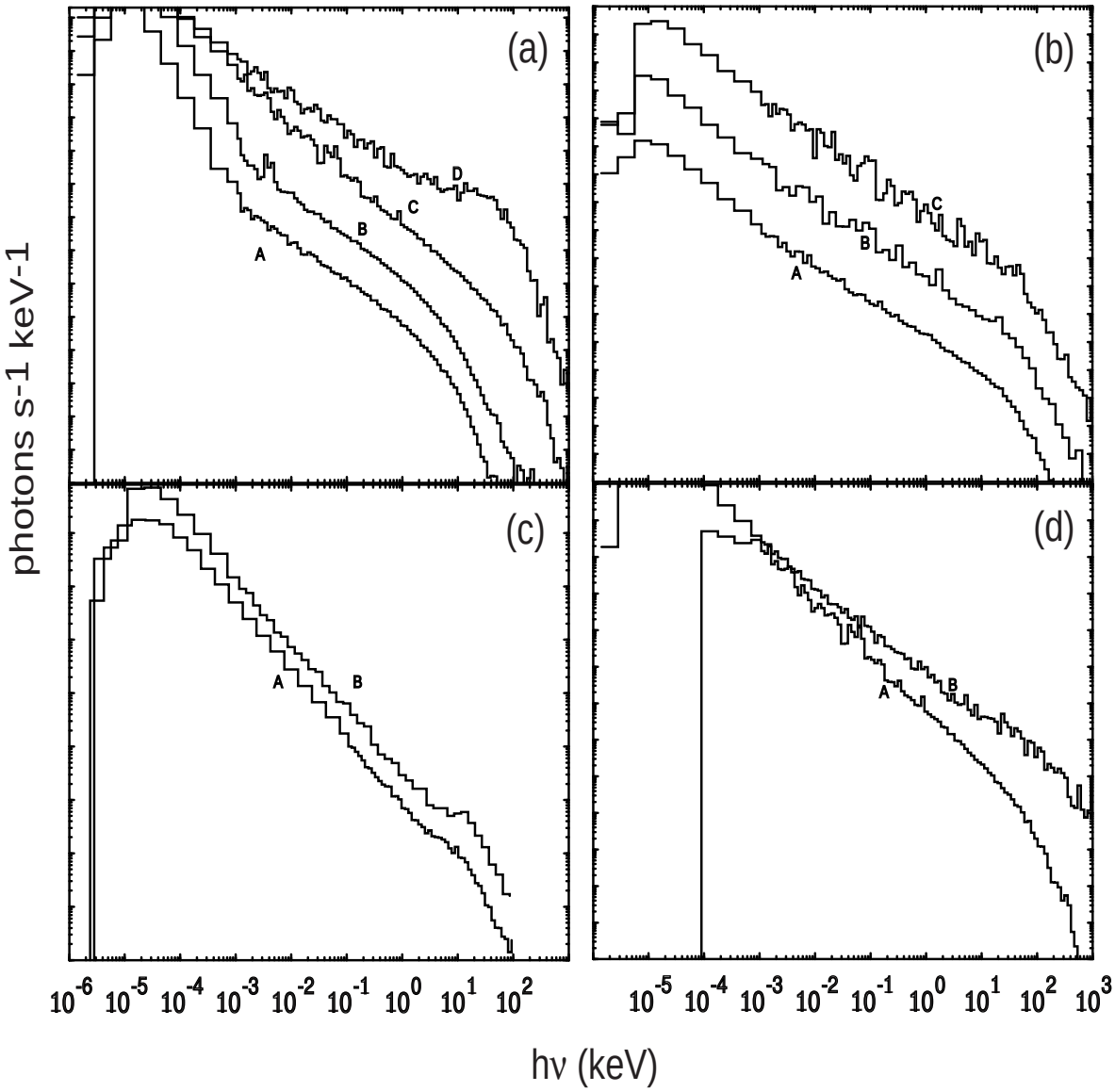
(a)
(b)
(c)
(d)
A
B
C
D
photons s-1 keV-1
hν (keV)
10-6 10-5 10-4 10-3 10-2 10-1 100 101 102
10-5 10-4 10-3 10-2 10-1 100 101 102 103

Radius	R	=	8.5×10^{16} cm d_9 $\Phi_{200}^{1/2}$ $\tau_{20}^{-1/2}$
Bulk Lorentz factor	Γ	$\geq$	376 $d_9^{1/2}$ $\Phi_{200}^{1/4}$ $\tau_{20}^{-1/4}$ $\Delta T_{10}^{-1/2}$
Total lepton number	N_e	=	2.7×10^{60} d_9^2 Φ_{200} $\Omega_{4\pi}$
Total lepton Mass	M_e	=	2.5×10^{33} gm d_9^2 Φ_{200} $\Omega_{4\pi}$
Total shell mass	M	=	M_e $f_p \equiv M_e(1 + 1836\frac{n_p}{n_e}) \leq 1837 M_e$
Total bulk kinetic energy	M Γ c^2	$\geq$	8.5×10^{56} ergs $d_9^{5/2}$ $\Phi_{200}^{5/4}$ $\tau_{20}^{-1/4}$ $\Omega_{4\pi}$ f_p $\Delta T_{10}^{-1/2}$
Blastwave transition radius	R_{BW}	$\equiv$	$(\frac{3\ M}{4\pi\ \Omega_{4\pi}\ m_H\ n_{ISM}})^{1/3} = 7.1 \times 10^{18}$ cm $d_9^{2/3}$ $\Phi_{200}^{1/3}$ $f_p^{1/3}$ $n_{ISM}^{-1/3}$
Blastwave transition time	T_{BW}	$\equiv$	$\frac{R_{BW}}{2\Gamma^2 c} \leq 837$ sec $d_9^{-1/3}$ $\Phi_{200}^{-1/6}$ $\tau_{20}^{1/2}$ $f_p^{1/3}$ ΔT_{10} $n_{ISM}^{-1/3}$

Table 1: Parameters of the GRB ejecta shell based on the saturated Compton model (scaled to the spectral parameters of the first ROTSE interval). Here $d_9 \times 9$ Gpc is the distance to the burster, $\Phi_{200} \equiv \Phi_0/200$, $\tau_{20} \equiv \tau_T/20$, $T_{10} \times 10$ sec is the pulse rise time in the detector frame, $\Omega_{4\pi}$ is the shell angular filling factor divided by 4π, n_p/n_e is the ratio of ejecta protons to leptons, and n_{ISM} is the ISM density in cm^{-3}.